

Stability and Bifurcation of Longitudinal Vehicle Braking

B.J. Olson* (olsonbr1@egr.msu.edu) and S.W. Shaw† (shawsw@egr.msu.edu)
Michigan State University

G. Stépan‡ (stepan@mm.bme.hu)
Budapest University of Technology and Economics and Hungarian Academy of Sciences

November 17, 2004

Abstract.

The longitudinal braking dynamics of a two-wheel vehicle model on an incline are considered using techniques from nonlinear dynamics. The model is planar and incorporates the coupled dynamics of two independently braked wheels and the vehicle body, and takes into account the slip dynamics of each wheel. By using the wheel slip values and the vehicle speed as dynamic states, it is shown that the qualitative behavior of the system can be completely captured by studying a relatively simple phase plane problem described in terms of the slip values. A systematic bifurcation analysis is carried out in which the brake torques of the two wheels are varied, and it is shown how the system transitions from stable braking to the possibility of lockup in one or both wheels, to guaranteed lockup in both wheels. In this manner a quite complete picture of the dynamic behavior is obtained as a function of the two brake torques, including regions with multiple possible steady braking outcomes, depending on the initial conditions. This analysis provides new insights into the dynamics of vehicle braking, and it provides a correction to the standard result for the critical values of the brake torques at which the wheels undergo lockup. This approach may also prove useful for evaluating brake proportioning schedules, or for investigating anti-lock braking systems and other methods of traction control.

Keywords: bifurcation, lockup instability, traction, vehicle braking, wheel slip

Abbreviations: ABS – Antilock Brake System; TCS – Traction Control System

1. Introduction

In a previous paper the authors considered the nonlinear dynamics of vehicle traction (braking and acceleration) of a single-wheel, or quarter-car model [1]. It was shown that the dynamics are conveniently captured by a system in which the vehicle speed and the wheel slip are taken as the independent dynamic states, in contrast to the usual approach, which utilizes vehicle speed and wheel rotational speed for states. This approach provides a model in which the existence, stability, and bifurcation of steady braking (resp. acceleration) conditions are easily interpreted using a single function that depends on the vehicle parameters, the slip, and the brake (resp. engine) torque. The primary parameter considered in the bifurcation analysis was the brake (resp. engine)

* Address correspondence to: B.J. Olson, Department of Mechanical Engineering, Michigan State University, East Lansing, MI 48824, USA. Phone: (517) 432-1085, Fax: (517) 353-1750.

† Department of Mechanical Engineering, Michigan State University, East Lansing, MI 48824, USA. Phone: (517) 432-3920, Fax: (517) 353-1750. Visiting Professor, Department of Mechanical Engineering, University of California – Santa Barbara.

‡ Department of Applied Mechanics, Budapest University of Technology and Economics, Budapest, Hungary. Phone: +36 1 463 1369, Fax: +36 1 463 3471.



torque acting on the wheel, and it was shown that, depending on the level of this torque and on the initial conditions, the vehicle could exhibit stable braking (resp. acceleration), wheel lockup (resp. “break-loose”), or a state of hysteresis in which both conditions coexist. This approach offers a quite complete picture of the system behavior and its dependence on system parameters and initial conditions. An important outcome of that study was a stability result related to brake lockup. Specifically, it was shown that the standard result for the critical level of the brake torque at which lockup occurs [2] is only an approximation that is valid in a parameter range that is valid for most passenger vehicles. Furthermore, the precise lockup condition was determined, showing how the standard result is obtained by the approximation.

The present study extends this line of analysis to a two-wheel, or half-car vehicle model that moves longitudinally on an incline relative to gravity. A standard formulation for the tire/road interaction is adopted, in which the longitudinal force acting on the wheel, that is, the braking force, is proportional to the normal load acting on the contact patch and to a coefficient of friction that depends in a nonlinear manner on the relative slip [2, 3]. The slip is a dimensionless measure of the difference between the forward vehicle speed and the circumferential speed of the wheel relative to its center, and its presence is required for a tractive force to be generated. The equations of motion are first formulated in their natural manner using the vehicle speed and the front and rear wheel speeds as dynamic states. These equations are converted to the desired form using the definition of slip, resulting in a set of three differential equations that describe the longitudinal dynamics of the overall vehicle and the slip dynamics of the two wheels. It should be noted that this model is valid for transient behavior, although the emphasis of the present analysis is on steady braking conditions.

An important feature of this model is that the vehicle speed appears in a manner that allows it to be essentially uncoupled from the slip dynamics, resulting in a phase plane system that captures the qualitative behavior of the two-wheel model. In this planar system it is shown that two relatively simple functions can completely describe the entire dynamics of the overall system. These two functions—one each for the front and rear slip states—depend on the system geometric and physical parameters, the slip values, and the brake torques. A detailed investigation of the functions and of the associated phase planes is carried out, capturing the entire range of system behaviors for a range of front and rear brake torques. In this manner it is determined how the system dynamics change via bifurcations as the brake torques are varied, including the transition from stable braking to possible and/or guaranteed lockup in one or both wheels.

The paper is outlined as follows. In order to motivate the two-wheel model, a review of the single-wheel braking model is given in Section 2 with emphasis on its tractive properties and a particular choice of dynamic states. The governing equations of motion are then derived and global features of the single-wheel system response are discussed. The stability and bifurcation of the slip dynamics are described, and the new condition for the lockup instability is reviewed. Some new results are also offered in this section, including an estimate of the stopping time. Section 3 contains the main results of the paper. It begins with a derivation of the two-wheel dynamic model, expressed in terms of the slip dynamics, which accounts for dynamic load transfer and for motion on an incline. A detailed analysis is carried out for this model, showing the entire range of system responses and the bifurcations that relate them, as a function of the two independent brake torques. The results

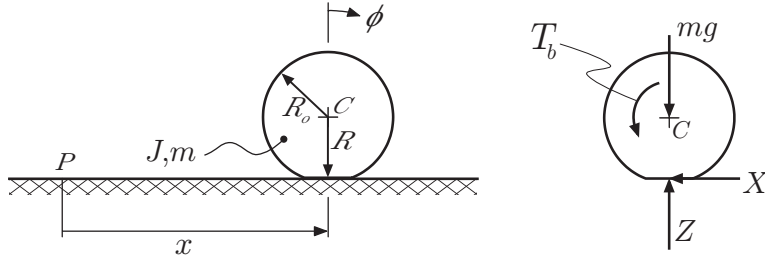


Figure 1. Schematic of the single-wheel braking model and corresponding free body diagram.

include an estimate of the stopping time and new conditions for the lockup instability thresholds for both front and rear wheels. The paper closes with conclusions and directions for future work.

2. Review of the Single-Wheel Braking Model

Single-wheel braking and acceleration models were considered in detail in a previous study [1]. The essential features of the former are reviewed here, as they are essential for the analysis of the two-wheel braking model of Section 3.

The single-wheel braking model, which is shown in Figure 1, consists of a single wheel of radius R_o that moves longitudinally with a speed $u(t) = \dot{x}(t)$ and absolute rotational rate $\omega(t) = \dot{\phi}(t)$. The longitudinal brake force X is sustained by the brake torque $T_b > 0$ and the reaction force Z balances the static weight mg of the wheel. The equations of motion follow from Newton's equations and are given by

$$\left. \begin{aligned} m\dot{u} &= -X \\ 0 &= Z - mg \\ J\dot{\omega} &= RX - T_b \end{aligned} \right\}, \quad (1)$$

where m , R , and J are the mass, effective rolling radius, and polar moment of inertia of the wheel,¹ and g is the acceleration due to gravity. Overdots denote differentiation with respect to time.

This model includes the longitudinal brake force X (which is discussed in the next section) as the only means of deceleration. Other sources of deceleration include driveline drag, grade, rolling resistance, and aerodynamic drag [2, 3], but are not considered here. See [4] for the effects of rolling resistance and aerodynamic drag on the structure of equations of motion.

2.1. TRACTIVE PROPERTIES

The friction coupling between the tire and road surface is captured by the friction law

$$X = \mu(s)Z, \quad (2)$$

where $\mu(s) \geq 0$ is an experimentally derived friction characteristic [5–7]. It depends on wheel slip, which is a dimensionless measure of the difference between the vehicle speed u and the

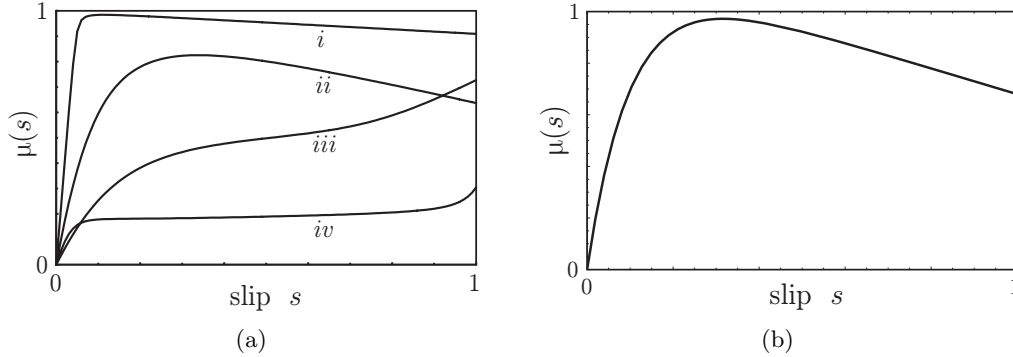


Figure 2. (a) Typical longitudinal friction characteristics: (i) Dry asphalt; (ii) Wet asphalt; (iii) Gravel; (iv) Packed snow. (b) The friction characteristic employed in the numerical simulations.

circumferential speed ωR of the wheel relative to its center. Wheel slip [2, 3, 5] is defined on the unit interval $I = [0, 1]$ in terms of this difference as

$$s \equiv \frac{u - \omega R}{u}, \quad s \in I, \quad (3)$$

where it is taken as convention that $u > 0$ and $0 \leq \omega R \leq u$ during braking.

Zero slip, i.e. $s = 0$, implies (1) $u = \omega R \neq 0$, or (2) $u = \omega R \equiv 0$, which corresponds to static equilibrium. The former is possible as an initial condition with $T_b > 0$ or for free rolling in the steady-state with $T_b = 0$. But since $T_b > 0$ by convention, zero slip is allowed only as an initial condition. Thus, there are two possible cases for steady-state braking with nonzero initial speed:

1. Finite rotation of the wheel ($\omega R \neq 0$) while the vehicle decelerates with $s \in (0, 1)$;
2. Deceleration under lockup conditions ($\omega R = 0$) with $s = 1$.

The longitudinal friction characteristic $\mu(s)$ is empirically derived in terms of road test data [6, 7], and functions are selected to fit these data.² One such function is the so-called *magic formula* of Pacejka [8, 9], which is given by

$$y(x) = D \sin(C \arctan(Bx - E(Bx - \arctan(Bx)))). \quad (4)$$

Equation (4) can be used to represent other steady-state tire characteristics in addition to the longitudinal friction characteristic. The physical parameters B , C , D , and E are chosen accordingly.

Figure 2a shows some typical representations of $\mu(s)$ for various road surfaces. Wet and dry asphalt characteristics are distinguished by a single local maximum on I , typically between 10 and 20% slip. That is, they are *unimodal* in s . The friction characteristics for gravel and packed snow are qualitatively different, with peak values at $s = 1$, or wheel lockup. In these cases the plowing action of the tire yields the dominant braking effect [5, 6].

The current study focuses on unimodal friction characteristics, although the techniques are applicable to any form of $\mu(s)$. To this end, and for efficient numerical simulations, a simple function

was devised for the friction characteristic and is given by

$$\mu(s) = 1.18 \left(1 - e^{-10s}\right) - s/2, \quad s \in I. \quad (5)$$

Equation (5), which is shown in Figure 2b, is employed for all calculations involving $\mu(s)$ for the single-wheel braking model and for the two-wheel braking model of Section 3. Note that this model has a peak value of $\mu_p = \mu(s_p) = 0.972$, which occurs at $s = s_p = 0.316$.

2.2. EQUATIONS OF MOTION

For general braking conditions the single-wheel model has two dynamic states and there are three possible dynamic variables to describe its motion, namely, u , ω , and s . It is quite natural and common to describe the dynamics in terms of the physically obvious variables, that is, the forward vehicle speed and the wheel's absolute rotational rate. Liu and Sun [10] have developed the equations of motion for a single-wheel model in this way, but their investigation focuses on control algorithms based on gain scheduling, rather than general dynamic behavior. In terms of u and ω , the equations of motion are given by

$$\dot{u} = -g\mu(s), \quad (6a)$$

$$\dot{\omega} = \frac{mgR\mu(s) - T_b}{J} = \frac{g}{R}(\nu\mu(s) - \Upsilon_b). \quad (6b)$$

Here, ν and Υ_b are a dimensionless inertia ratio and a nondimensional brake torque, and are defined as follows:

$$\nu = \frac{mR^2}{J}$$

$$\Upsilon_b = \frac{R}{Jg}T_b$$

Note that the speeds u and ω are coupled in a complicated way via the wheel slip. An alternative approach is to take u and s as dynamic states, instead of u and ω [1]. It will be shown that this allows for a simple geometric interpretation of the system dynamics for the entire range of vehicle speeds and slip values, and that a single function in s captures these dynamics.

Evaluating the time rate of change of wheel slip and performing the appropriate substitutions, the dynamic equations are found to be

$$\left. \begin{aligned} \dot{u} &= -\mu(s)g \\ \dot{s} &= \frac{g}{u}h_b(s) \end{aligned} \right\}, \quad u \in \mathbb{R}_+, \quad s \in I, \quad (7)$$

where, recall, $I = [0, 1]$ and $\mathbb{R}_+ = (0, \infty)$ denotes the set of positive real numbers. The dimensionless function

$$h_b(s) = (s - 1 - \nu)\mu(s) + \Upsilon_b \quad (8)$$

depends on wheel slip as well as the dimensionless inertia and torque parameters defined above. The dynamic equations of motion given by Equation (7) are also coupled, but in a less cumbersome manner that will be exploited below.

Next we show that there exist slip values that are invariant under the dynamics, and we characterize their stability. Steady braking occurs when s lies on a stable invariant value and u simply decreases towards zero (since $\dot{u} < 0$ during braking), that is, the vehicle decelerates under constant wheel slip. Global features of the single-wheel braking model, including its transient response, are reviewed in Section 2.4.

2.3. STEADY SLIP CONDITIONS AND LOCAL STABILITY

Assuming that the brake torque Υ_b is constant (or slowly varying), one may view Equation (7) as a second-order autonomous system. It is clear that the system does not possess equilibria of the form $(u, s) = (u^*, s^*)$. This would require $\mu(s^*) = 0$, which is a condition that is satisfied only for $s = s^* = 0$. (See Figure 2b.) As discussed in Section 2.1, zero slip is possible only if the brake torque is zero or if the vehicle is in static equilibrium, both of which violate the assumption that braking is occurring. Steady values of slip (denoted $s = s^*$) may exist and are geometrically constrained to the unit interval $I = [0, 1]$. However, since dynamic wheel slip is restricted to $s \in (0, 1]$, the steady slip values, when they exist, may be either on the boundary at $s = 1$, denoted *boundary equilibria*, or in the interior region corresponding to $s \in (0, 1)$, denoted *interior equilibria*. (While these are not equilibria for the overall dynamic system, they are equilibria for the s -dynamics, as described below.) The interior equilibria, if they exist, must satisfy

$$h_b(s^*) = (s^* - 1 - \nu)\mu(s^*) + \Upsilon_b = 0. \quad (9)$$

(We ignore the nonphysical $u \rightarrow \infty$ case.) It is important to note that this condition depends only on s and the system parameters. Boundary equilibria will occur when $h_b(1) \geq 0$, implying that the torque is sufficient to drive s to unity. In this case there is a boundary equilibrium at $s^* = s^L = 1$. In fact, by uncoupling the s -dynamics, the behavior of this system can be completely captured by a one-dimensional dynamical system, as follows. If time is rescaled according to

$$t = \frac{u}{g}\tau \quad (10)$$

then the s -dynamics are governed by

$$s' = h_b(s), \quad s \in I, \quad (11)$$

where $(\cdot)' = \frac{\partial(\cdot)}{\partial\tau}$. In the formulation given by Equation (11) the s -dynamics behave quite simply but its parameterization with respect to time continually varies as u decreases. The rescaled time τ is simply a (nonuniformly) stretched out version of the real time t . Once the s -dynamics are known, the rather trivial u -dynamics can be simply determined.

Local stability of the interior equilibria can be obtained by considering a small perturbation $\eta(\tau) = s(\tau) - s^*$ away from s^* . Then Equation (11) can be locally approximated to leading order

by the linearized equation

$$\eta'(\tau) = \left. \frac{\partial h_b}{\partial s} \right|_{s^*} \eta(\tau). \quad (12)$$

Equation (12) shows that the perturbation grows exponentially fast when $\frac{\partial h_b}{\partial s}(s^*) > 0$ and decays exponentially when $\frac{\partial h_b}{\partial s}(s^*) < 0$. We therefore define

$$\left. \begin{aligned} s^a &= \{s \mid h_b(s^a) = 0, \frac{\partial h_b}{\partial s}(s^a) < 0\} \\ s^r &= \{s \mid h_b(s^r) = 0, \frac{\partial h_b}{\partial s}(s^r) > 0\} \end{aligned} \right\}, \quad (13)$$

which are stable and unstable interior equilibria, respectively. Here, the superscript a denotes stable, or *attracting*, and r denotes unstable, or *repelling*.

An examination of the function $h_b(s)$ indicates that s^r exists only if $h_b(1) \geq 0$. This condition also implies the existence of the boundary equilibrium at $s^* = s^L = 1$, which is unstable when $h_b(1) = 0$ and stable when $h_b(1) > 0$. In fact, s^r and s^L are born in a saddle-node bifurcation at a brake torque level $\Upsilon_b = \nu\mu(1)$.

The boundary and interior equilibria s^* define invariant manifolds in the (u, s) state space, and this holds when time is rescaled back to its physical source. These are given by

$$\mathcal{W}_b^* = \{(u, s) \mid u \geq 0, s = s^*\}, \quad (14)$$

where $*$ denotes a (attracting), r (repelling), or L (lockup). Note that \mathcal{W}_b^a and \mathcal{W}_b^r are the system nullclines.

2.4. GLOBAL FEATURES OF THE SINGLE-WHEEL BRAKING MODEL

2.4.1. State-Space Description

The longitudinal motion of the vehicle is governed by $\dot{u} = -\mu(s)g$ (see Equation 7), which shows that its deceleration is directly proportional to the slip-dependent friction generated between the tire and the road. The slip dynamics are governed by $\dot{s} = \frac{g}{u}h_b(s)$ and are coupled to the longitudinal vehicle dynamics via u , which appears only in the denominator. Since $\dot{s} \sim \frac{1}{u}$, the transient slip dynamics evolve at a rate that increases with decreasing u .

The function $h_b(s)$, which is given by Equation (8), plays a central role in the stability and bifurcation of the slip dynamics. As discussed in Section 2.3, the zeros of $h_b(s^*)$ (given implicitly by Equation 9) define possible steady slip values (equilibria in s), and hence the invariant manifolds \mathcal{W}_b^* , while the sign of $\frac{\partial h_b}{\partial s}(s^*)$ characterizes their stability. Given the inertia ratio ν and a particular brake torque Υ_b , Equation (8) can be used to qualitatively construct the (u, s) phase plane, as follows.

Figure 3 shows a plot of $h_b(s)$ and the corresponding state space description in u and s for $\nu = 15$ and $\Upsilon_b = 12$. At these parameter values there are stable and unstable interior equilibria at $s^a = 0.117$ and $s^r = 0.782$, which define the stable and unstable invariant manifolds \mathcal{W}_b^a and \mathcal{W}_b^r , respectively. Since $h_b(1) > 0$, $s^L = 1$ is also an attracting invariant slip value, which defines the invariant manifold \mathcal{W}_b^L .

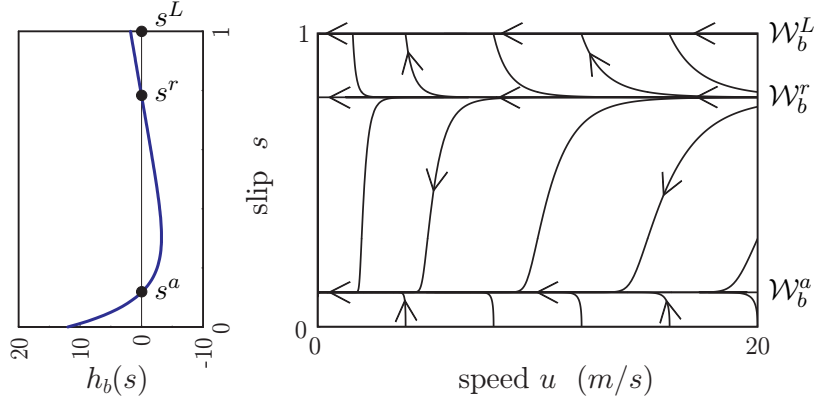


Figure 3. $h_b(s)$ versus s and the corresponding state space description in u and s for $\nu = 15$ and $\Upsilon_b = 12$.

The set of all initial conditions that yield stable braking is the domain of attraction of $s^* = s^a$ and is given by

$$\mathcal{S} = \{(u, s) \mid u > 0, s \in [0, s^r]\}. \quad (15)$$

Trajectories started in \mathcal{S} rapidly approach the stable invariant manifold and essentially evolve along \mathcal{W}_b^a towards zero vehicle (and wheel) speed. The set of all initial conditions that yield braking under lockup conditions is the domain of attraction of $s^* = s^L = 1$, which is given by

$$\mathcal{L} = \{(u, s) \mid u > 0, s \in (s^r, 1]\}. \quad (16)$$

Trajectories started in \mathcal{L} tend rapidly to lockup at $s = 1$ (actually reaching lockup in finite time due to the discontinuous nature of the vector field at the boundary) and evolve along \mathcal{W}_b^L towards zero vehicle speed. Initial conditions started on the unstable invariant manifold monotonically evolve along \mathcal{W}_b^r towards zero speed at the point $(u, s) = (0, s^r)$. This situation, however, is not physically realizable since the manifold is locally unstable.

The entire range of dynamics are captured in the bifurcation diagram shown in Figure 4, which is a plot of the interior and boundary equilibria s^* (including their stability types) as a function of the dimensionless brake torque for $\nu = 15$. This classical hysteresis diagram is generated by following the zeros of $h_b(s)$, and also the boundary equilibria when $h_b(1) \geq 0$, as the brake torque parameter Υ_b is increased. (Note that Υ_b is simply additive.) As the brake torque increases from zero, the steady slip value increases from zero and is initially stable. It destabilizes at point a , which corresponds to a saddle-node bifurcation of s^a and s^r (captured by the condition where $h_b(s)$ has a degenerate zero), and jumps to lockup at $s^* = s^L = 1$. This occurs at a critical brake torque designated as Υ_b^{cr} . Note that the stable lockup condition $s^* = s^L = 1$ and the unstable slip value s^r appear in another saddle node bifurcation at a lower brake torque, designated as b in Figure 4. (This is not a saddle-node bifurcation in the classical sense. However, we shall regard the birth/annihilation of equilibria on the boundary as such here and in Section 3.3 when discussing the global features of the two-wheel braking model.) In order to restore stable braking, the brake

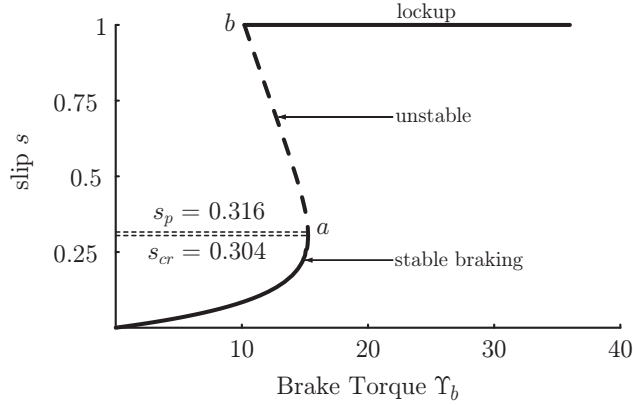


Figure 4. Bifurcation diagram for the single-wheel braking model for $\nu = 15$.

torque must be reduced to a value corresponding to point b , where the slip jumps back to the lower stable branch.

The features described here assume a constant brake torque Υ_b , while in practice the brake torque is generally time-dependent. It is important to note, however, that the qualitative results of this section (and also Section 3.3 where the global features of a two-wheel braking model are discussed) remain valid even for $\Upsilon_b = \Upsilon_b(t)$, provided that it is slowly varying. Varying the brake torque amounts to shifting the stable and unstable manifolds \mathcal{W}_b^a and \mathcal{W}_b^r simultaneously while the slip and speed dynamics evolve. The slip dynamics either remain at lockup or “track” the stable invariant manifold \mathcal{W}_b^a , while the speed dynamics simply decrease to zero, essentially independent of the slip dynamics. A suddenly (instantaneously) applied brake torque is dynamically equivalent to imposing an initial condition of zero slip and some positive initial speed. For brake torques that vary at a rate that is comparable to the time-evolution of the slip, there may be other dynamics to consider.

2.4.2. Lockup Instability and Critical Brake Torque

The level of the brake torque at which lockup is impending is of particular interest. The standard textbook result [2, 3, 5] is that Υ_b can be increased until wheel slip reaches s_p —which corresponds to the maximum value of the friction characteristic—beyond which lockup occurs. The corresponding critical brake torque is assumed to be

$$T_b^{cr}|_{\text{approx}} = mgR\mu(s_p),$$

which is the maximum moment that can be provided by the friction force $X = \mu(s_p)Z = \mu(s_p)mg$ about the wheel center (assuming that s_p can be reached). In dimensionless notation, the assumed critical brake torque is given by

$$\Upsilon_b^{cr}|_{\text{approx}} = \nu\mu(s_p). \quad (17)$$

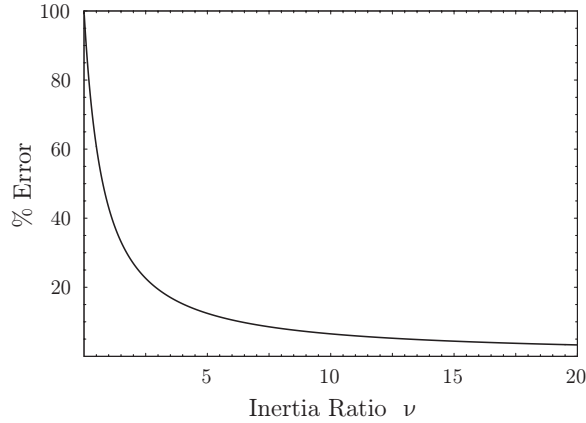


Figure 5. Percent error between the actual (Eqn. 18) and approximate (Eqn. 17) critical brake torques as a function of the vehicle-to-wheel inertia ratio ν .

It was shown in [1] that Equation (17) is only an approximation to the actual critical brake torque, which occurs at the saddle-node bifurcation at point a in Figure 4. It is given by

$$\Upsilon_b^{cr} = \nu\mu(s_{cr}) \left[1 + \frac{1}{\nu} (1 - s_{cr}) \right], \quad (18)$$

where $s_{cr} < s_p$ corresponds to the point at which the saddle-node bifurcation occurs. Thus, the assumed critical brake torque follows from two related assumptions:

1. The vehicle-to-wheel inertia ratio ν is large relative to unity;
2. The lockup instability occurs at $s_p > s_{cr}$.

For typical passenger vehicles the assumed critical brake torque is a good approximation, and its accuracy increases for decreasing ν . Figure 5 shows a plot of the percent error

$$\% \text{ Error} = \left(\frac{\Upsilon_b^{cr} - \Upsilon_b^{cr}|_{\text{approx}}}{\Upsilon_b^{cr}} \right) \times 100\% \quad (19)$$

between Equation (18) and Equation (17) in terms of the inertia ratio ν . For example, taking $\nu = 15$ (a value for a typical passenger vehicle, and the value used in the simulations) yields an error of about 5%. However, the error can become quite substantial for vehicles with relatively large wheels.

To better understand the approximations involved in Equation (17) reconsider the governing equations of motion in terms of the longitudinal vehicle speed u and its absolute rotational rate ω , which are given by Equation (6). If the rotational inertia of the wheel is ignored, the equations reduce to

$$\dot{u} = -g\mu(s^*), \quad (20a)$$

$$0 = \frac{g}{R} (\nu\mu(s^*) - \Upsilon_b). \quad (20b)$$

The approximation given by Equation (17) follows from solving Equation (20b) for the required brake torque Υ_b and then maximizing the corresponding deceleration of the vehicle (Equation 20a) by setting $s^* = s_p$.

2.4.3. Stopping Time

Though it is generally not possible to extract the time dynamics directly from a phase plane diagram, it is possible to estimate them here since the slip dynamics are generally much faster than the vehicle speed dynamics. Consider the case when a brake torque $\Upsilon_b < \Upsilon_b^{cr}$ is suddenly applied to a vehicle moving at a forward speed of $u(t=0) = u_o > 0$. (This is a physically common situation.) Trajectories evolve from a condition of zero slip, i.e. $(u, s) = (u_o, 0)$, rapidly approach the stable invariant manifold, and then essentially evolve along \mathcal{W}_b^a towards zero speed according to

$$u(t) = u_o^a - \mu(s^a)g(t - t^a), \quad t^a \leq t \leq t_s, \quad (21)$$

where u_o^a is the speed at $t = t^a$ when the trajectory has essentially reached \mathcal{W}_b^a (for example, when it is within 2% of the limiting steady slip value s^a). The remaining time for the vehicle to come to rest at time t_s is

$$t_s - t^a = \frac{u_o^a}{\mu(s^a)g}, \quad (22)$$

which follows from setting $u(t_s) = 0$ in Equation (21). For reasonable initial speeds $u_o > 0$ the slip dynamics evolve much faster than the speed dynamics, and this rate increases for decreasing u . (Recall that $\dot{s} \sim \frac{1}{u}$.) Thus t^a is small, which implies $u_o^a \cong u_o$, and

$$t_s \cong \frac{u_o}{\mu(s^a)g} \quad (23)$$

gives a reasonable approximation of the time required for the vehicle to come to rest. This result is shown in Figure 6, where the approximate stopping time t_s is plotted in terms of the dimensionless brake torque Υ_b for $\nu = 15$ and for various initial speeds u_o . As expected, for $\Upsilon_b < \Upsilon_b^{cr}$, the stopping time increases for increasing u_o and decreasing Υ_b . For $\Upsilon_b > \Upsilon_b^{cr}$ the stopping time is

$$t_s^L \cong \frac{u_o}{\mu(1)g}, \quad (24)$$

which is independent of the brake torque since the vehicle is at lockup. The discontinuity of the estimated stopping time at $\Upsilon_b^{cr} = 15.250$ corresponds to the saddle-node bifurcation of the stable and unstable interior equilibria s^a and s^r (point a in Figure 4).

3. The Two-Wheel Braking Model

The two-wheel vehicle braking model to be considered is shown schematically in Figure 7. The entire weight Mg of the vehicle (including the wheels) is assumed to be concentrated at its mass center, which is located a length c forward of the rear axle and a distance h normal to the road surface. The front and rear wheels are assumed to be identical, each with effective rolling radius

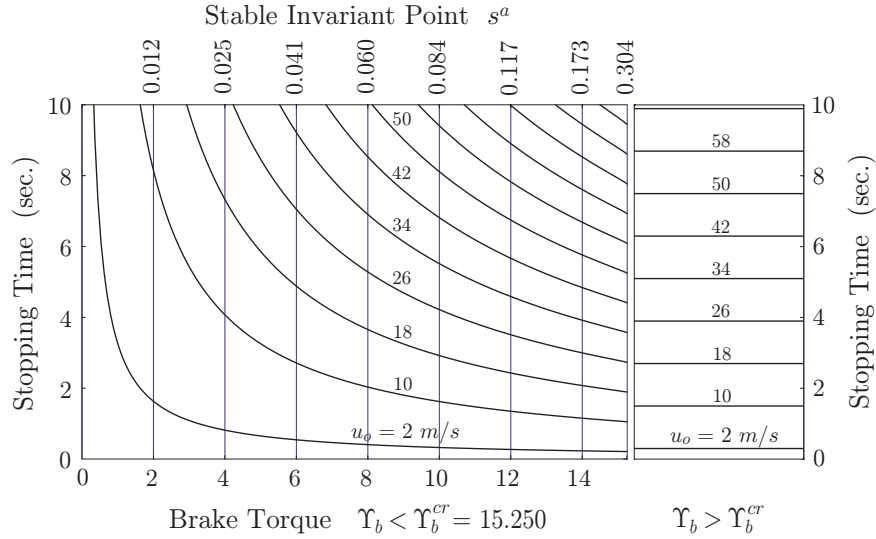


Figure 6. Approximate stopping time for $\nu = 15$ and for various brake torques Υ_b and initial speeds u_o .

R and polar moment of inertia J . Their centers are separated by a distance $l = b + c$. The vehicle moves longitudinally in the x -direction at a rate $u(t) = \dot{x}(t)$ along the road surface, which is inclined at an angle θ with respect to the horizontal. The friction coupling between the rear and front wheels and the road surface is captured by the brake (friction) forces X_r and X_f , respectively, and the normal forces on the rear and front wheels are denoted by Z_r and Z_f , respectively. The brake torques $T_{bi} > 0$ ($i = r, f$), which sustain the friction forces X_i , are independently generated by rear and front braking mechanisms. The system is planar, that is, lateral motions, cornering, etc., are not considered. Moreover, the effects of driveline and aerodynamic drag, rolling resistance, etc., on the vehicle deceleration are not incorporated into the model.

The dynamic equations of motion follow from Newton's equations. By summing forces in the x - and z -directions, moments about the mass center of the vehicle and the mass centers of the rear and front wheels, it follows that

$$\left. \begin{aligned} M\dot{u} &= Mg \sin \theta - X_r - X_f \\ 0 &= Mg \cos \theta - Z_r - Z_f \\ 0 &= h(X_r + X_f) + cZ_r - bZ_f \\ J\dot{\omega}_r &= RX_r - T_{br} \\ J\dot{\omega}_f &= RX_f - T_{bf} \end{aligned} \right\}, \quad (25)$$

where \dot{u} is the vehicle acceleration along the incline, $\dot{\omega}_i$ ($i = r, f$) are the absolute angular accelerations of the rear and front wheels, and g is the acceleration due to gravity.

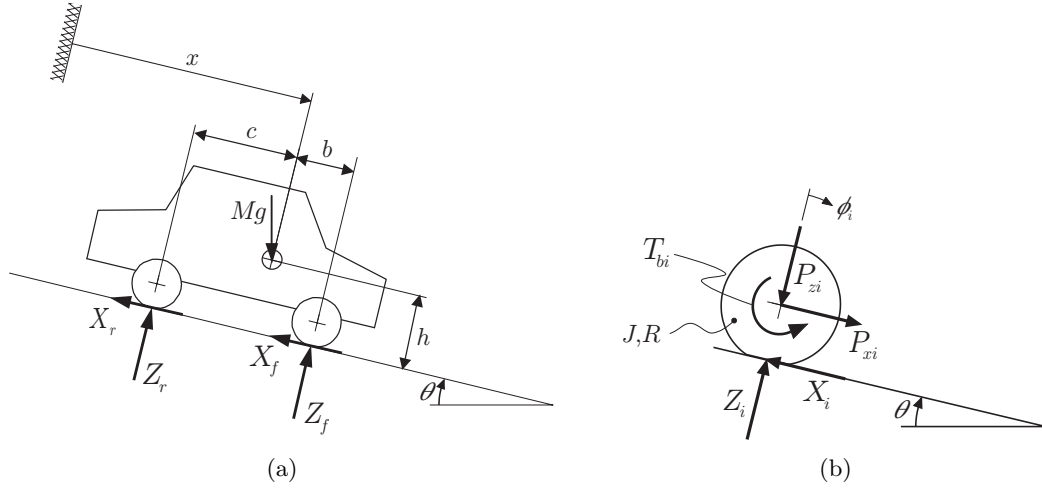


Figure 7. (a) Schematic and free body diagram of the two-wheel braking model and (b) corresponding free body diagram of the rear ($i = r$) and front ($i = f$) wheels.

As in the single-wheel model, the friction coupling to ground can be characterized in terms of wheel slip. Each wheel is assumed to obey the friction law given by Equation (2), that is,

$$X_i = \mu(s_i)Z_i \quad (i = r, f). \quad (26)$$

This friction model allows for independent dynamics of the rear and front wheels, but assumes identical friction characteristics between each wheel and the road. That is, the vehicle is assumed to travel on a homogeneous surface and the physical properties of each tire (construction, inflation, wear, etc.) are assumed to be the same.³ Rear and front slip are defined using Equation (3) as

$$s_i \equiv \frac{u - \omega_i R}{u}, \quad s_i \in I \quad (i = r, f), \quad (27)$$

where it is taken as convention that $u > 0$ and $0 \leq \omega_i R \leq u$.

The introduction of two independently rolling wheels in the vehicle braking model renders the front and rear reaction forces dynamic terms in the equations of motion; that is, they become acceleration dependent. This phenomenon is known as *dynamic load transfer* [2, 3] and is captured by the normal forces

$$\left. \begin{aligned} Z_r &= Mg \left(\frac{b}{l} \cos \theta - \frac{h}{l} \sin \theta \right) + M\dot{u} \frac{h}{l} \\ Z_f &= Mg \left(\frac{c}{l} \cos \theta + \frac{h}{l} \sin \theta \right) - M\dot{u} \frac{h}{l} \end{aligned} \right\} \quad (28)$$

acting on the tires, which follow from elimination of the braking forces X_i from the first three elements of Equation (25). The first terms on the right hand side of Equation (28) are recognized to be the static normal loads on the rear and front wheels, and the term $M\dot{u} \frac{h}{l}$ is defined as the *dynamic load transfer*. Since $\dot{u} < 0$, this term is negative for vehicle braking. Thus, in agreement with intuition, dynamic load transfer has the effect of shifting normal loads from the rear wheel to

the front wheel during braking. Of course, this affects the braking forces, which in turn affect the wheel speeds, wheel slip, etc., resulting in a complicated feedback that couples the system dynamics in a nontrivial manner.

Again, as in the single-wheel case, the dynamics become more transparent if one makes use of the slip dynamics. We now formulate the dynamic equations of motion in terms of the vehicle speed and the speeds of the rear and front wheels and then convert them to the desired form in terms of wheel slip.

3.1. EQUATIONS OF MOTION

For general braking conditions, the two-wheel model possesses three dynamic states and hence requires a set of three independent coordinates to describe its motion. In terms of the physically obvious variables, namely the forward vehicle speed and the absolute rotational rate of each wheel, the equations of motion are determined by eliminating the forces X_i and Z_i ($i = r, f$) from the seven conditions given by Equation (25) and Equation (26), and then solving for the vehicle and wheel accelerations. The result is

$$\dot{u} = -g(\Lambda_b(\mathbf{s}) \cos \theta - \sin \theta), \quad (29a)$$

$$\dot{\omega}_r = \frac{MgR\mu(s_r) \left(\frac{b}{l} - \Lambda_b(\mathbf{s}) \frac{h}{l} \right) \cos \theta - T_{br}}{J} = \frac{g}{R} (\nu\mu(s_r)\lambda_r(\mathbf{s}) - \Upsilon_{br}), \quad (29b)$$

$$\dot{\omega}_f = \frac{MgR\mu(s_f) \left(\frac{c}{l} + \Lambda_b(\mathbf{s}) \frac{h}{l} \right) \cos \theta - T_{bf}}{J} = \frac{g}{R} (\nu\mu(s_f)\lambda_f(\mathbf{s}) - \Upsilon_{bf}), \quad (29c)$$

where $\mathbf{s} = (s_r, s_f)$ is a vector and

$$\nu = \frac{MR^2}{J},$$

$$\Upsilon_{bi} = \frac{R}{Jg} T_{bi} \quad (i = r, f)$$

are the vehicle-to-wheel inertia ratio and rear and front dimensionless brake torques. The functions

$$\left. \begin{aligned} \lambda_r(\mathbf{s}) &= \left(\frac{b}{l} - \Lambda_b(\mathbf{s}) \frac{h}{l} \right) \cos \theta \\ \lambda_f(\mathbf{s}) &= \left(\frac{c}{l} + \Lambda_b(\mathbf{s}) \frac{h}{l} \right) \cos \theta \end{aligned} \right\} \quad (30)$$

are nondimensional dynamic normal loads on the rear and front wheels and

$$\Lambda_b(\mathbf{s}) = \frac{\mu(s_r) \frac{b}{l} + \mu(s_f) \frac{c}{l}}{1 + \frac{h}{l} (\mu(s_r) - \mu(s_f))} \quad (31)$$

is a dimensionless measure of the vehicle acceleration along the incline. An example plot of $\Lambda_b(\mathbf{s})$ is shown in Figure 8. For $h/l = 0.125$, $c/l = 0.6$, and $b/l = 0.4$ it has a peak value of $\Lambda_b^p = \Lambda_b(\mathbf{s}_p) =$

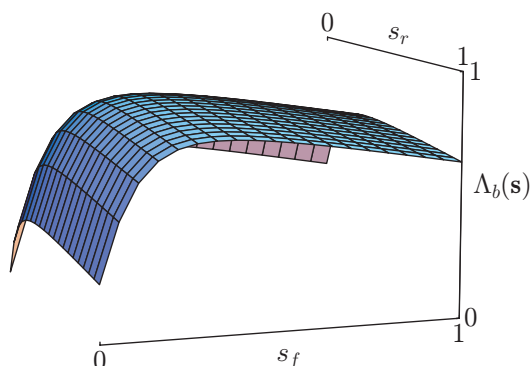


Figure 8. The function $\Lambda_b(\mathbf{s})$ for $h/l = 0.125$, $c/l = 0.6$, and $b/l = 0.4$.

0.972 at $\mathbf{s}_p = (s_p, s_p) = (0.316, 0.316)$. Since $\Lambda_b(\mathbf{s})$ depends only on the vehicle geometry and the friction characteristics $\mu(s_i)$ between each tire/wheel and the road surface, it can be regarded as an effective friction characteristic for the two-wheel braking model. Finally, note that Equation (31) reduces to $\mu(s)$ when $s_r = s_f = s$, i.e., $\Lambda_b(s, s) = \mu(s)$.

The speeds u , ω_r , and ω_f in Equation (29) are coupled in a complicated way via the slip variables s_r and s_f . An alternative formulation of the equations of motion follows from replacing the angular speeds ω_i with the slip variables s_i as dynamic states. It will be shown that such a formulation allows for a fairly simple geometric interpretation of the system dynamics for the entire range of slip values, and that two functions in \mathbf{s} capture these dynamics.

Evaluating the time rate of change of each s_i and performing the appropriate substitutions, the equations of motion for the two-wheel system are found to be

$$\left. \begin{aligned} \dot{u} &= -g(\Lambda_b(\mathbf{s}) \cos \theta - \sin \theta) \\ \dot{\mathbf{s}} &= \frac{g}{u} \mathbf{h}_b(\mathbf{s}) \end{aligned} \right\}, \quad u \in \mathbb{R}_+, \quad \mathbf{s} \in I^2, \quad (32)$$

where the elements of $\mathbf{h}_b(\mathbf{s}) = (h_{br}(\mathbf{s}), h_{bf}(\mathbf{s}))$ are defined in detail below, $I^2 = I \times I$ is the unit square, and the term $\Lambda_b(\mathbf{s})$ is given by Equation (31). The dimensionless functions $h_{br}(\mathbf{s})$ and $h_{bf}(\mathbf{s})$ are the generalization of $h_b(s)$ for the single-wheel braking model of Section 2 and play a central role in the slip dynamics of the two-wheel braking model. They are given by

$$h_{bi}(\mathbf{s}) = (s_i - 1)(\Lambda_b(\mathbf{s}) \cos \theta - \sin \theta) - \mu(s_i) \nu \lambda_i(\mathbf{s}) + \Upsilon_{bi} \quad (i = r, f). \quad (33)$$

Example plots of $h_{br}(\mathbf{s})$ and $h_{bf}(\mathbf{s})$ are shown in Figure 9 for $\theta = 0$, $\nu = 15$, $\Upsilon_{br} = 3.5$, $\Upsilon_{bf} = 10.0$, and for a particular vehicle geometry.

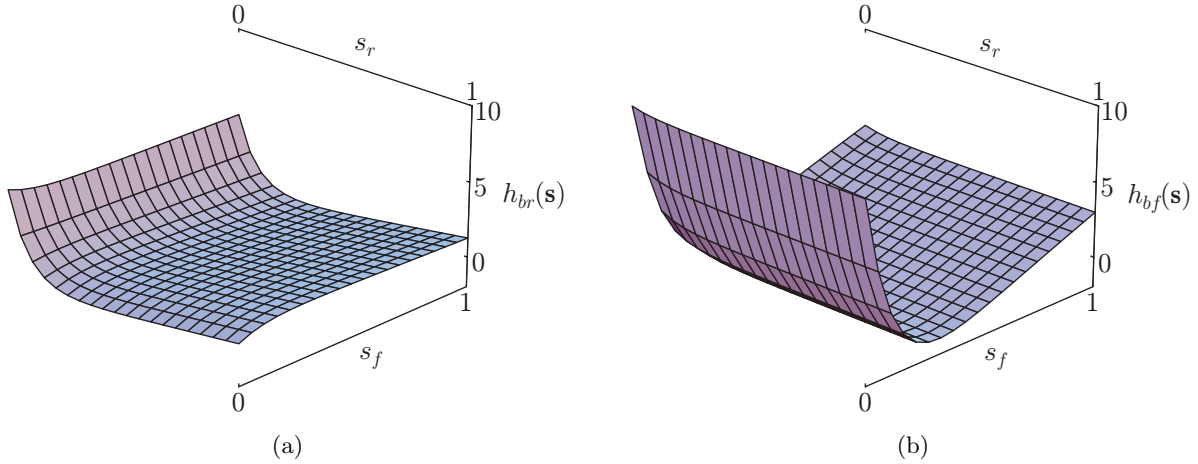


Figure 9. The functions $h_{bi}(\mathbf{s})$ ($i = r, f$) for $h/l = 0.125$, $c/l = 0.6$, $b/l = 0.4$, $\theta = 0$, $\nu = 15$, $\Upsilon_{br} = 3.5$, and $\Upsilon_{bf} = 10.0$: (a) $h_{br}(\mathbf{s})$; (b) $h_{bf}(\mathbf{s})$.

3.2. SLIP DYNAMICS OF THE TWO-WHEEL BRAKING MODEL

The relationship between slip values s_i ($i = r, f$) and the vehicle speed becomes clear by invoking a Leibniz notation scheme, forming the ratio of \dot{s}_r to \dot{s}_f , and invoking Equation (32). Then

$$\frac{ds_r}{ds_f} = \frac{\dot{s}_r}{\dot{s}_f} = \frac{\frac{g}{u} h_{br}(\mathbf{s})}{\frac{g}{u} h_{bf}(\mathbf{s})} = \frac{h_{br}(\mathbf{s})}{h_{bf}(\mathbf{s})}, \quad (34)$$

which shows that relative changes in rear and front slip are a function of the ratio of $h_{br}(\mathbf{s})$ to $h_{bf}(\mathbf{s})$ and are *invariant* to changes in the vehicle speed. It therefore suffices to investigate the *planar system*

$$\dot{\mathbf{s}} = \frac{g}{u} \mathbf{h}_b(\mathbf{s}), \quad \mathbf{s} \in I^2, \quad u \in \mathbb{R}_+ \quad (35)$$

and study the slip dynamics on the unit square I^2 . Note that if time is rescaled according to

$$t = \frac{u}{g} \tau \quad (36)$$

then Equation (35) becomes

$$\left. \begin{aligned} s'_r &= h_{br}(\mathbf{s}) \\ s'_f &= h_{bf}(\mathbf{s}) \end{aligned} \right\}, \quad \mathbf{s} \in I^2, \quad (37)$$

where $(\cdot)' = \frac{\partial(\cdot)}{\partial\tau}$. Equation (37) is also a planar system, but its parameterization with respect to time continually varies as u decreases. In fact, the rescaled time τ depends monotonically on the real time t , but is (nonuniformly) stretched out by an amount that depends on the instantaneous vehicle speed.

We begin the analysis in the next section by establishing the existence of steady slip solutions, which define invariant manifolds in the (u, \mathbf{s}) space. Local stability of these steady slip values is covered in Section 3.2.2 and their bifurcation is discussed in Section 3.3.

3.2.1. Steady Slip Conditions

Assuming that the brake torques Υ_{br} and Υ_{bf} are constant or slowly varying, the slip dynamics of the two-wheel model are governed by a second-order autonomous system, which is given by Equation (37), and these dynamics are geometrically constrained to the unit square I^2 . As in the single-wheel case, zero slip in one or both wheels is not considered in the braking model. Thus, there are four possible cases for steady-state braking with nonzero vehicle speed:

1. Rotation of both the rear and front wheels ($\omega_r R \neq 0$ and $\omega_f R \neq 0$) with $(s_r, s_f) \in (0, 1) \times (0, 1)$;
2. Finite rotation of the rear wheel ($\omega_r R \neq 0$) and lockup of the front wheel ($\omega_f R = 0$) with $s_r \in (0, 1)$ and $s_f = 1$;
3. Lockup of the rear wheel ($\omega_r R = 0$) and finite rotation of the front wheel ($\omega_f R \neq 0$) with $s_r = 1$ and $s_f \in (0, 1)$;
4. Lockup of both the rear and front wheels ($\omega_r R = \omega_f R = 0$) with $s_r = s_f = 1$.

The equilibria, if they exist, may be either on the boundary at $s_r = 1$ and/or $s_f = 1$, denoted *boundary equilibria*, or in the interior region corresponding to $\mathbf{s} \in (0, 1) \times (0, 1)$, denoted *interior equilibria*.

The interior equilibria $\mathbf{s}^* = (s_r^*, s_f^*)$, if they exist, must satisfy

$$0 = \mathbf{h}_b(\mathbf{s}^*), \quad (38)$$

that is,

$$h_{bi}(\mathbf{s}^*) = (s_i^* - 1) (\Lambda_b(\mathbf{s}^*) \cos \theta - \sin \theta) - \mu(s_i^*) \nu \lambda_i(\mathbf{s}^*) + \Upsilon_{bi} = 0 \quad (i = r, f). \quad (39)$$

Given values for the front and rear brake torques Υ_{bi} , Equation (39) defines possible steady slip pairs $\mathbf{s}^* = (s_r^*, s_f^*)$ in the interior of I^2 that are invariant under the dynamics. All combinations of \mathbf{s}^* , if they exist, define invariant sets of the two-wheel system. Specifically, if the system states lie on such an invariant set, the dynamics are quite simple: the slip values remain constant and the vehicle speed monotonically decreases accordingly. In order to quantify these steady slip pairs, it is convenient to define the following sets

$$\begin{aligned} \mathcal{H}_i^a &= \left\{ \mathbf{s} \mid h_{bi}(\mathbf{s}) = 0, \frac{\partial h_{bi}}{\partial s_i}(\mathbf{s}) < 0 \right\} \quad (i = r, f), \\ \mathcal{H}_i^r &= \left\{ \mathbf{s} \mid h_{bi}(\mathbf{s}) = 0, \frac{\partial h_{bi}}{\partial s_i}(\mathbf{s}) > 0 \right\} \quad (i = r, f), \end{aligned}$$

which are the system nullclines. The sets \mathcal{H}_r^a and \mathcal{H}_r^r consist of all slip pairs $\mathbf{s} = (s_r, s_f)$ such that the surface $h_{br}(\mathbf{s})$ (see Figure 9a) intersects the plane $\mathbf{h}_b = 0$ with negative and positive slopes,

Table I. (a) Interior equilibria and (b) boundary equilibria and their stability types. For an invariant point $\mathbf{s}^{(p k)}$, p indicates rear-slip stability and k indicates front-slip stability; a denotes stable, or *attracting*, r denotes unstable, or *repelling*, and L denotes lockup.

(a) Interior Equilibria			(b) Boundary Equilibria		
Letter	\mathbf{s}^*	Stability Type	Letter	\mathbf{s}^*	Stability Type
A	$\mathbf{s}^{(a a)} = \mathcal{H}_r^a \cap \mathcal{H}_f^a$	Stable Node	E	$\mathbf{s}^{(a L)} = \mathcal{H}_r^a \cap \mathcal{L}_f$	Stable Node
B	$\mathbf{s}^{(a r)} = \mathcal{H}_r^a \cap \mathcal{H}_f^r$	Saddle	F	$\mathbf{s}^{(r L)} = \mathcal{H}_r^r \cap \mathcal{L}_f$	Saddle
C	$\mathbf{s}^{(r a)} = \mathcal{H}_r^r \cap \mathcal{H}_f^a$	Saddle	G	$\mathbf{s}^{(L a)} = \mathcal{L}_r \cap \mathcal{H}_f^a$	Stable Node
D	$\mathbf{s}^{(r r)} = \mathcal{H}_r^r \cap \mathcal{H}_f^r$	Unstable Node	H	$\mathbf{s}^{(L r)} = \mathcal{L}_r \cap \mathcal{H}_f^r$	Saddle
			I	$\mathbf{s}^{(L L)} = \mathcal{L}_r \cap \mathcal{L}_f$	Stable Node

respectively, in the s_r -direction. The sets \mathcal{H}_f^a and \mathcal{H}_f^r are similarly defined in terms of the function $h_{bf}(\mathbf{s})$ (see Figure 9b) and its slope along the s_f -axis. While these sets do not immediately determine the stability of equilibria, they are very useful for organizing the various equilibria, and we offer a conjecture about their relation to stability at the end of the next subsection.

The interior equilibria of the two-wheel system are defined by the intersections of the sets \mathcal{H}_i^a and \mathcal{H}_i^r , and are summarized in Table I(a). The superscripted pair of letters on \mathbf{s} indicate local stability, which is considered in Section 3.2.2. For convenience, the nine possible (interior and boundary) equilibria \mathbf{s}^* are assigned arabic letters A-I.

Physically, once the rear (resp. front) wheel experiences lockup at a given brake torque Υ_{br} (resp. Υ_{bf}) with the front (resp. rear) brake torque fixed, the rear (resp. front) slip remains at $s_r = 1$ (resp. $s_f = 1$), even if Υ_{br} (resp. Υ_{bf}) is increased or decreases slightly (due to hysteresis). Thus the boundary equilibria, if they exist, must be contained in the sets

$$\mathcal{L}_i = \{\mathbf{s} \mid s_i = 1, 0 \leq s_j \leq 1\} \quad (i = r, f \text{ and } j = f, r)$$

and are defined by the intersections of the sets \mathcal{L}_i with \mathcal{H}_i^a and \mathcal{H}_i^r ($i = r, f$). These equilibria are summarized in Table I(b). (The superscript L on \mathbf{s} denotes lockup.)

Figure 10a shows an example plot of the sets \mathcal{H}_i^a , \mathcal{H}_i^r , and \mathcal{L}_i for $\theta = 0$, $\nu = 15$, $\Upsilon_{br} = 3.4$, $\Upsilon_{bf} = 9.0$, and for a particular vehicle geometry. Figure 10b shows the corresponding state space description of the two-wheel model slip dynamics, indicating the boundary and interior equilibria \mathbf{s}^* . These steady slip pairs define invariant manifolds in the (u, \mathbf{s}) phase space, which are given by

$$\mathcal{V}_b^* = \{(u, \mathbf{s}) \mid u \geq 0, \mathbf{s} = \mathbf{s}^*\}. \quad (40)$$

Here, $*$ denotes a (attracting), r (repelling), or L (lockup).

3.2.2. Local Stability of Slip Dynamics

Local stability of the slip dynamics, which are described by Equation (37), can be obtained by considering small perturbations $\eta_i(\tau) = s_i(\tau) - s_i^*$ away from the invariant points s_i^* ($i = r, f$).

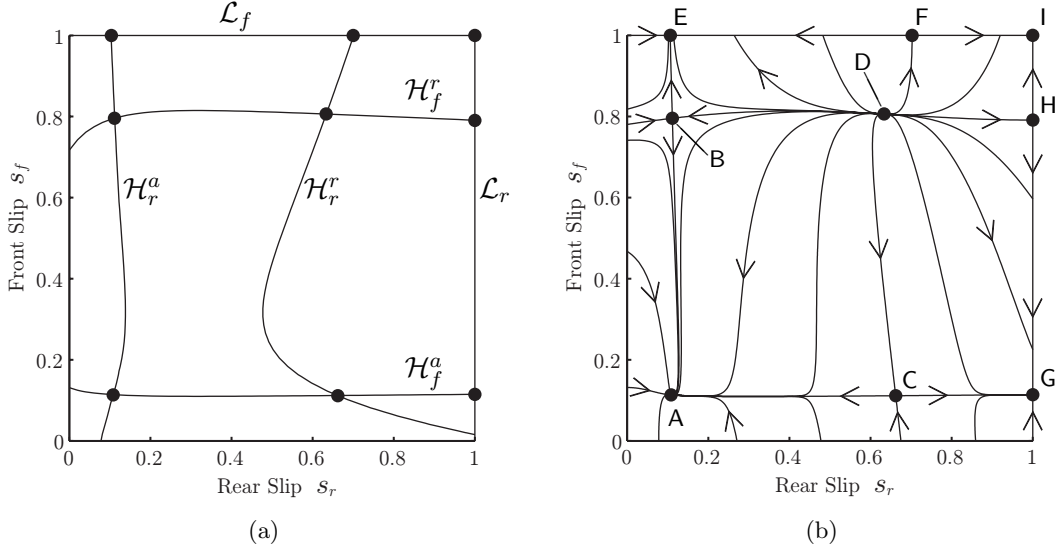


Figure 10. (a) The system nullclines \mathcal{H}_i^a , \mathcal{H}_i^r , and the sets \mathcal{L}_i ($i = r, f$); (b) the corresponding state space description of the slip dynamics of the two-wheel model for $h/l = 0.125$, $c/l = 0.6$, $b/l = 0.4$, $\theta = 0$, $\nu = 15$, $\Upsilon_{br} = 3.4$, and $\Upsilon_{bf} = 9.0$.

Then the local stability of the interior equilibria $\mathbf{s}^* = (s_r^*, s_f^*)$ follows from the linearized equation

$$\boldsymbol{\eta}'(\tau) = \left. \frac{\partial \mathbf{h}_b}{\partial \mathbf{s}} \right|_{\mathbf{s}^*} \boldsymbol{\eta}(\tau), \quad (41)$$

where $\boldsymbol{\eta} = (\eta_r, \eta_f)$ is a vector and

$$\frac{\partial \mathbf{h}_b}{\partial \mathbf{s}} = \begin{bmatrix} \frac{\partial h_{br}}{\partial s_r} & \frac{\partial h_{br}}{\partial s_f} \\ \frac{\partial h_{bf}}{\partial s_r} & \frac{\partial h_{bf}}{\partial s_f} \end{bmatrix} \quad (42)$$

is the Jacobian matrix. Given the scalar functions $h_{bi}(\mathbf{s})$, one need only check the eigenvalues $\sigma_{1,2}$ of $\left. \frac{\partial \mathbf{h}_b}{\partial \mathbf{s}} \right|_{\mathbf{s}^*}$ to determine the local stability of each invariant point \mathbf{s}^* in the interior of I^2 .

Since the system is planar, classification of the interior equilibria can also be determined from conditions on the trace and determinant

$$\mathcal{T} \equiv \text{tr} \left(\frac{\partial \mathbf{h}_b}{\partial \mathbf{s}} \right) = \frac{\partial h_{br}}{\partial s_r} + \frac{\partial h_{bf}}{\partial s_f}, \quad (43a)$$

$$\mathcal{D} \equiv \det \left(\frac{\partial \mathbf{h}_b}{\partial \mathbf{s}} \right) = \frac{\partial h_{br}}{\partial s_r} \frac{\partial h_{bf}}{\partial s_f} - \frac{\partial h_{br}}{\partial s_f} \frac{\partial h_{bf}}{\partial s_r}, \quad (43b)$$

of the Jacobian matrix, as outlined in [11]. In terms of \mathcal{T} and \mathcal{D} , the eigenvalues are given by

$$\sigma_{1,2} = \frac{1}{2} \left(\mathcal{T} \pm \sqrt{\mathcal{T}^2 - 4\mathcal{D}} \right).$$

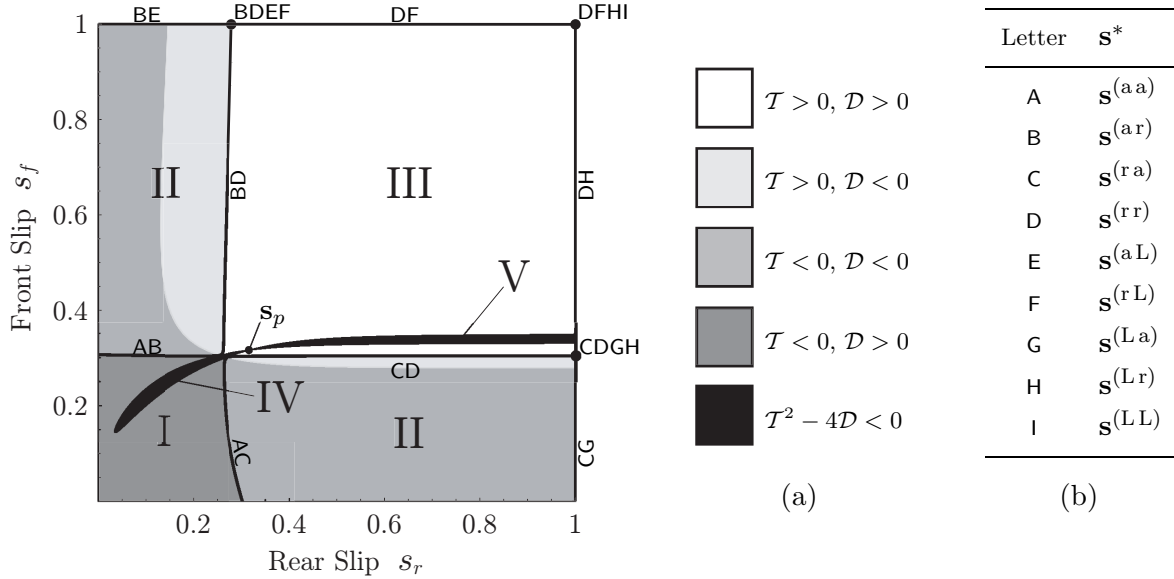


Figure 11. Stability diagram for the interior equilibria of the two-wheel braking model in terms of front and rear slip values s_f and s_r for $h/l = 0.2$, $c/l = 0.6$, $b/l = 0.4$, $\theta = 0$, and $\nu = 15$: (I) Stable nodes; (II) Saddle points; (III) Unstable nodes; (IV) Stable foci; (V) Unstable foci. (a) Conditions on \mathcal{T} and \mathcal{D} ; (b) Equilibria. The point $\mathbf{s}_p = (s_p, s_p) = (0.316, 0.316)$ corresponds to the peak of $\Lambda_b(\mathbf{s})$, which is shown in Figure 8 for the same vehicle geometry. Note that $\mathcal{T}^2 - 4\mathcal{D} > 0$ everywhere in I^2 except in the black regions IV and V.

One need only find the sign of the trace \mathcal{T} and determinant \mathcal{D} (and if $\mathcal{D} > 0$, the sign of $\mathcal{T}^2 - 4\mathcal{D}$) evaluated at $\mathbf{s} = \mathbf{s}^*$ in order to determine local stability of the interior equilibria. While it is a simple matter to find the signs of the diagonal terms of the Jacobian matrix evaluated at $\mathbf{s} = \mathbf{s}^*$ (and hence the sign of the trace \mathcal{T}) by inspection of the surfaces $h_{bi}(\mathbf{s})$ in Figure 9, it is not a simple matter to find the signs of its off-diagonal terms (which are needed to find \mathcal{D}) without numerically calculating them. We are thus reduced to numerically determining the stability of the interior equilibria. The results are summarized in Figure 11 for $\theta = 0$, $\nu = 15$, and for a particular vehicle geometry. Here, we wish only to note that Figure 11 indicates the signs of \mathcal{T} and \mathcal{D} and also the regions corresponding to particular stability types. This plot is valid for all values of the brake torques since they are simple additive terms in the functions h_{bi} . As these torques vary, the equilibria move in the this plane and have the stability types indicated.

The equilibrium point A is restricted to Region I (where $\mathcal{T}^2 - 4\mathcal{D} > 0$) and Region IV (where $\mathcal{T}^2 - 4\mathcal{D} < 0$), where $\mathcal{T} < 0$ and $\mathcal{D} > 0$. Thus A is either a stable node or a stable focus, and is denoted by $\mathbf{s}^{(aa)}$.⁴ The equilibrium point D is restricted to Region III (where $\mathcal{T}^2 - 4\mathcal{D} > 0$) and Region V (where $\mathcal{T}^2 - 4\mathcal{D} < 0$), where both the trace \mathcal{T} and determinant \mathcal{D} are positive; hence it is either an unstable node or an unstable focus and is denoted by $\mathbf{s}^{(rr)}$. The equilibrium points B and C are saddles since they are restricted to Region II, where $\mathcal{D} < 0$ and $\mathcal{T} \neq 0$. The invariant point B is attracting in rear slip and repelling in front slip, while C is repelling in rear slip and attracting in front slip. They are denoted by $\mathbf{s}^{(ar)}$ and $\mathbf{s}^{(ra)}$, respectively.

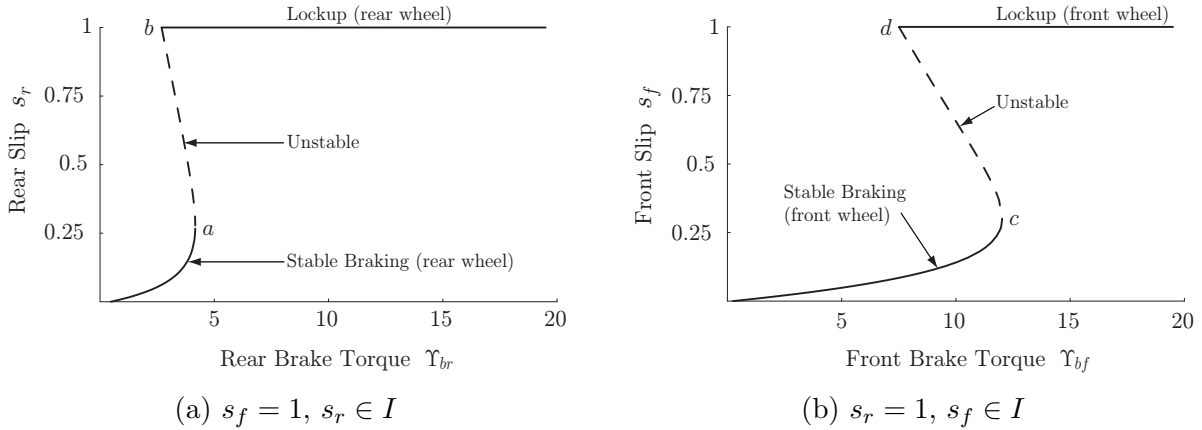


Figure 12. Bifurcation diagram for the boundary equilibria of the two-wheel braking model for $\nu = 15$: (a) front lockup; (b) rear lockup.

The stability types of the boundary equilibria are also determined numerically and are summarized in Figure 11 and Figure 12. These bifurcation diagrams show the steady rear (Fig. 12a) and front (Fig. 12b) slip conditions, respectively, while the front and rear wheels, respectively, are held locked, and as their respective brake torques are varied. Point a in Figure 12a corresponds to a saddle node bifurcation of the invariant points E and F, while point b corresponds to a saddle node bifurcation of the invariant points F and I. (See Table I or Figure 11b.) Similarly, points c and d in Figure 12b correspond to saddle node bifurcations involving the invariant points G, H, and I. Since the equilibrium points E, I, and G are attracting in both rear and front slip,⁵ they are stable nodes and are denoted by $\mathbf{s}^{(aL)}$, $\mathbf{s}^{(LL)}$, and $\mathbf{s}^{(La)}$, respectively. The equilibrium point F (resp. H) is repelling (resp. attracting) in rear (resp. front) slip and attracting (resp. repelling) in front (resp. rear) slip; it is therefore a saddle point and is denoted by $\mathbf{s}^{(rL)}$ (resp. $\mathbf{s}^{(Lr)}$).

As a final note, we conjecture (without proof) that the local stability of the interior and boundary equilibria $\mathbf{s} = \mathbf{s}^*$ follows unambiguously from the sets \mathcal{H}_i^a , \mathcal{H}_i^r , and \mathcal{L}_i that define them, where a denotes *attracting* and r denotes *repelling*. A summary of this claim is given in Table I. For example, the invariant set $\mathbf{s}^{(ar)} = \mathcal{H}_r^a \cap \mathcal{H}_f^r$ is attracting in rear slip and repelling in front slip, i.e., it is a saddle node. The invariant set $\mathbf{s}^{(La)} = \mathcal{L}_r \cap \mathcal{H}_f^a$ is attracting in both front and rear slip, i.e., it is a stable node.

3.3. GLOBAL FEATURES OF THE TWO-WHEEL BRAKING MODEL

Just as the dynamics of the single-wheel braking model can be characterized in terms of a single function $h_b(s)$, the dynamics of the two-wheel braking model are similarly characterized by the two functions $h_{br}(\mathbf{s})$ and $h_{bf}(\mathbf{s})$. These functions, which are given by Equation (33), define the steady slip values, and hence the invariant manifolds along which trajectories must evolve towards zero vehicle speed.

The bifurcation diagram depicted in Figure 13 contains the main results of this study. It shows the possible operating regimes of the two-wheel braking model in terms of the front and rear brake

Table II. Torque data for Figure 14.

Subfigure	Region	Υ_{br}	Υ_{bf}
(a)	III_a	1.5	13.0
(b)	IV_a	3.0	13.0
(c)	V	4.5	13.0
(d)	II_a	2.0	9.0
(e)	II	3.5	9.0
(f)	IV_b	5.0	9.0
(g)	I	2.5	5.0
(h)	II_b	4.0	5.0
(i)	III_b	5.5	5.0

torques for a model with $\theta = 0$, $\nu = 15$, and for a particular vehicle geometry. The front brake torque Υ_{bf} is defined along the ordinate while the rear brake torque Υ_{br} is defined along the abscissa. The diagram is separated into nine major regions of interest, which are denoted by the roman numerals I – V with subscripts. Figure 14 shows example phase portraits for these nine regions in terms of rear and front slip dynamics. (The corresponding torque values are given in Table II.) As mentioned above and shown in Table I and Figure 11b, the steady slip pairs $\mathbf{s}^* = (s_r^*, s_f^*)$ have been assigned arabic letters A–I. The general locations of these points and their stability types are indicated in Figure 13 and Table I.

Each curve in Figure 13 corresponds to a co-dimension one saddle-node bifurcation in the slip dynamics. For example, the line AC corresponds to a bifurcation involving the birth/annihilation of the stable node $\mathbf{s}^{(aa)}$ (point A) and the saddle point $\mathbf{s}^{(ra)}$ (point C). The lines involving the boundary equilibria E, F, G, H, or I are essentially saddle-node bifurcations where slip equilibria are either created or destroyed at the boundary of I^2 in the sets \mathcal{L}_r and \mathcal{L}_f . (Recall that trajectories are physically constrained to the unit square. Mathematically, trajectories are allowed outside of I^2 , but physically they are not.) By following the creation and destruction of various equilibria, the following features of the bifurcation diagram can be determined.

In region I the system possesses a single stable invariant point A. For brake torque values in this region, all initial conditions $\mathbf{s} \in I^2$ yield stable braking, with trajectories tending to the stable node $\mathbf{s}^{(aa)}$ (point A). Regions II_a and II_b are characterized by the coexistence of stable braking in both wheels with the possibility of lockup in one wheel, either the front (in II_a) or rear (in II_b). The braking outcome in these cases depends on the initial slip conditions. Region II is characterized by the coexistence of stable braking in both wheels with the possibility of front and/or rear lockup, depending on the initial conditions; that is, all four combinations of stable braking/lockup can be realized in this region. For brake torque pairs $(\Upsilon_{br}, \Upsilon_{bf})$ in Region III_a , all trajectories started in I^2 tend towards $\mathbf{s}^{(aL)}$ (point E), while in Region III_b trajectories tend towards $\mathbf{s}^{(La)}$ (point G). These cases correspond, respectively, to front (resp. rear) lockup with stable braking in the rear (resp. front) wheel. Brake torque values in Region IV_a (resp. Region IV_b) yield guaranteed lockup in the front (resp. rear) wheel and the possibility of the rear (resp. front) wheel undergoing either stable

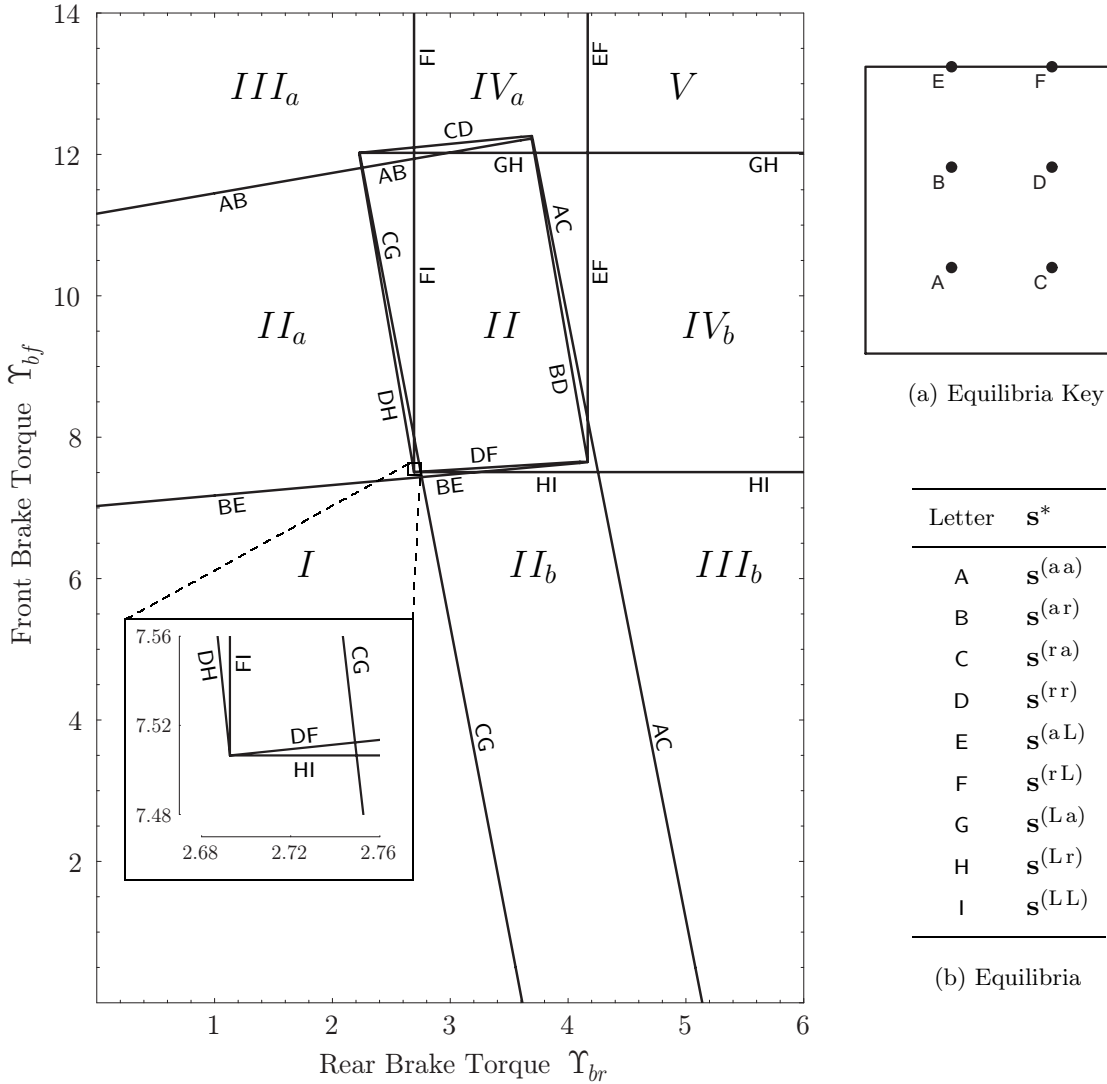


Figure 13. Bifurcation diagram for the two-wheel braking model in terms of the brake torques Υ_{br} and Υ_{bf} for $h/l = 0.2$, $c/l = 0.6$, $b/l = 0.4$, $\theta = 0$, and $\nu = 15$. (a) Equilibria locations; (b) Equilibria types.

braking (point E [resp. G]) or lockup (point I), depending on initial conditions. Finally, Region V consists of guaranteed lockup in both wheels with all trajectories tending to the stable node $\mathbf{s}^{(LL)}$ (point I).

There are a number co-dimension two bifurcation points in Figure 13 at which two saddle-node bifurcations are coincident. The first occurs at $(\Upsilon_{br}, \Upsilon_{bf}) \cong (2.6927, 7.5065)$, where the lines DH, FI, DF, and HI mutually terminate. (This is shown in the closeup view in the lower left-hand corner of the bifurcation diagram.) Similarly, the lines CG, DH, CD, and GH mutually terminate in a co-dimension two saddle-node bifurcation, as do the lines BD, EF, BE, and DF. The lines AB and BD

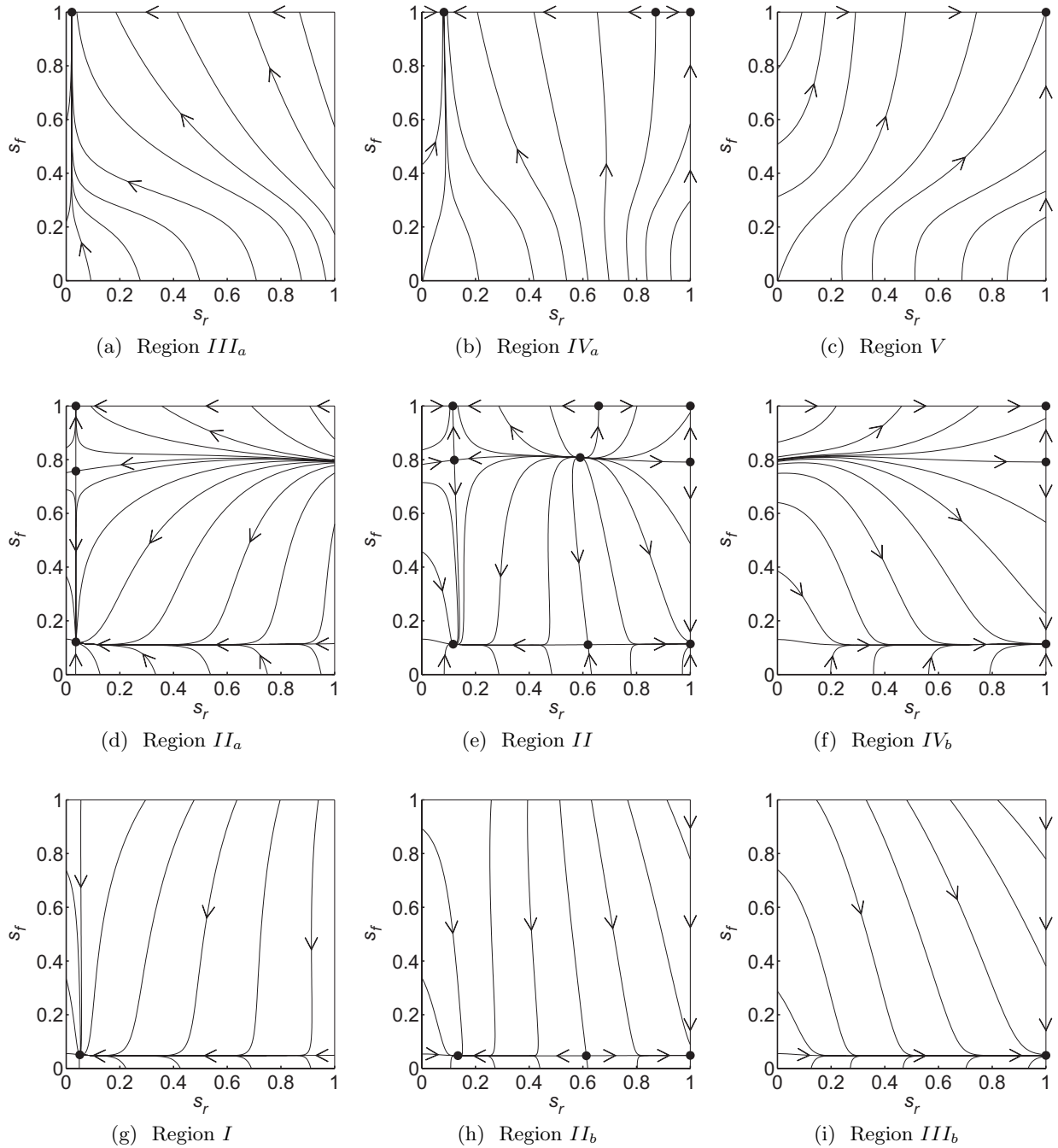


Figure 14. Example state space descriptions of the slip dynamics for $h/l = 0.2$, $c/l = 0.6$, $b/l = 0.4$, $\theta = 0$, and $\nu = 15$. Specific brake torque data are provided in Table II.

also mutually terminate in a bifurcation of the same type, as do the lines AC and CD, but it is not clear that these latter two bifurcations occur at the same point.⁶ The details in this region have not been resolved, but are partially explored below. It should be noted, however, that this region is not of practical interest since lockup of both wheels is imminent.

Figure 11 in Section 3.2.2 shows the slip pairs $\mathbf{s}^* = (s_r^*, s_f^*)$ that separate regions with different stability types. In terms of slip, the first three co-dimension two bifurcation points described above are indicated in this figure by the points BDEF, CDGH, and DFHI, which lie on the boundary of I^2 . The lines AB and BD mutually terminate at a point where $\mathcal{T} = 0$ near the slip pair (0.275, 0.300). The lines AC and CD similarly terminate in this slip region where $\mathcal{T} = 0$, but at a different point. That is, the four curves AB, BD, AC, and CD do not meet at a single point. There is a small region here that involves other bifurcations that correspond to the region of the torque pair (3.8, 12) in Figure 13, the details of which have not been resolved.

As a final note, the non-symmetric nature of Figure 11 and Figure 13 is due to dynamic load transfer. When a vehicle is braked, the dynamic normal load on the front wheels is greater by an amount that is directly proportional to the vehicle deceleration. This has the effect of reducing the available friction at the rear wheels. Thus the rear wheel experience lockup at a smaller brake torque than the front wheel.

To summarize, we stress that the dynamic behavior of the two-wheel system in braking is completely characterized by the two functions $h_{br}(\mathbf{s})$ and $h_{bf}(\mathbf{s})$ in which the dimensionless brake torques appear in an additive manner. For a particular set of dimensionless brake torques, one need only find the slip pairs $\mathbf{s}^* = (s_r^*, s_f^*)$ that make both $h_{br}(\mathbf{s})$ and $h_{bf}(\mathbf{s})$ vanish, along with the gradients of each of these functions in the s_r - and s_f -directions, respectively. With this knowledge, a qualitative description of the slip dynamics can be constructed. Figure 13 captures the essence of all possible operating regimes that can occur as the brake torques vary.

3.4. LOCKUP INSTABILITY AND CRITICAL BRAKE TORQUES

The brake torque levels at which lockup in one or both wheels is impending is of particular interest. It is typically assumed, as is done with the single wheel model, that the rear (resp. front) brake torque can be increased until the rear (resp. front) slip reaches s_p —which corresponds to the maximum value of the friction characteristic $\mu(s)$ —beyond which lockup occurs in the rear (resp. front) wheel. The corresponding assumed critical brake torques are [2]

$$\begin{aligned} T_{br}^{cr} |_{\text{approx}} &= MgR\mu(s_p) \left(\frac{b}{l} - \Lambda(\mathbf{s}_p) \frac{h}{l} \right) = MgR\mu(s_p) \lambda_r(\mathbf{s}_p), \\ T_{bf}^{cr} |_{\text{approx}} &= MgR\mu(s_p) \left(\frac{c}{l} + \Lambda(\mathbf{s}_p) \frac{h}{l} \right) = MgR\mu(s_p) \lambda_f(\mathbf{s}_p), \end{aligned}$$

where $\mathbf{s}_p = (s_p, s_p)$ corresponds to the peak value of the effective friction characteristic $\Lambda_b(\mathbf{s})$. In dimensionless notation, the assumed critical brake torques are given by

$$\Upsilon_{bi}^{cr} |_{\text{approx}} = \nu\mu(s_p) \lambda_i(\mathbf{s}_p) \quad (i = r, f), \quad (44)$$

where $\lambda_i(\mathbf{s})$ ($i = r, f$) are the dimensionless normal loads on the rear and front wheels. Equation (44) is an approximation to the actual critical brake torques, which we now consider.

A very common situation is for the brake torques to be applied *suddenly* to the front and rear wheels in which case trajectories evolve from $(u, s_r, s_f) = (u_o, 0, 0)$, where u_o is the vehicle speed at $t = t_o = 0$. For torque values in Region *I* of the bifurcation diagram shown in Figure 13, trajectories approach the stable invariant manifold $\mathcal{V}_b^{(aa)}$ (see Equation 40), which is defined by the stable node $\mathbf{s}^{(aa)}$ (point A), and stable braking is guaranteed. Brake torque values in Regions *II*, *II_a*, or *II_b* would still yield stable braking since trajectories evolve from a condition of zero slip, i.e., $(u, s_r, s_f) = (u_o, 0, 0)$. Specifically, the appearance of points B and E (resp. C and G) corresponds to the *possibility* of front (resp. rear) lockup, but since trajectories evolve from $(u, s_r, s_f) = (u_o, 0, 0)$, the outcome would still be stable braking. The actual limits on the brake torques are determined by examining the bifurcation conditions for which point A disappears, namely, lines AB and AC in Figure 13, beyond which lockup of the front and rear wheels occurs, respectively.⁷ Thus the conditions for lockup in the rear and front wheels follow from Equation (39) and are given by

$$\Upsilon_{br}^{cr} = \nu \left[\mu(s_r^{AC}) \lambda_r(\mathbf{s}^{AC}) + \frac{1}{\nu} (1 - s_r^{AC}) (\Lambda_b(\mathbf{s}^{AC}) \cos \theta - \sin \theta) \right], \quad (45)$$

$$\Upsilon_{bf}^{cr} = \nu \left[\mu(s_f^{AB}) \lambda_f(\mathbf{s}^{AB}) + \frac{1}{\nu} (1 - s_f^{AB}) (\Lambda_b(\mathbf{s}^{AB}) \cos \theta - \sin \theta) \right], \quad (46)$$

where $\mathbf{s}^{AC} = (s_r^{AC}, s_f^{AC})$ is the set of all slip pairs that correspond to saddle-node bifurcations of the interior equilibria $\mathbf{s}^{(aa)}$ and $\mathbf{s}^{(ra)}$ (line AC in Figure 11). The set $\mathbf{s}^{AB} = (s_r^{AB}, s_f^{AB})$ is similarly defined in terms of saddle-node bifurcations of the equilibria $\mathbf{s}^{(aa)}$ and $\mathbf{s}^{(ar)}$ (line AB in Figure 11).

The peak slip pair $\mathbf{s}_p = (s_p, s_p)$ is shown in Figure 11 for the same geometry parameters used in the bifurcation diagrams. It is contained in region *III*, which corresponds to unstable nodes and foci. Thus it is clearly impossible to maintain stable braking conditions at (or even near) the peak slip pair \mathbf{s}_p , which is assumed in the approximate brake torques given in Equation (44). From these considerations, it follows that the assumed critical brake torques are based on two related assumptions:

1. The vehicle-to-wheel inertia ratio ν is large relative to unity;
2. The lockup instability occurs at $\mathbf{s}_p = (s_p, s_p)$.

Further insight into these assumptions can be gained by reconsidering the governing equations of motion given by Equation (29), which are in terms of the longitudinal vehicle speed u and the absolute rotational rates ω_i of the rear and front wheels. If one ignores the rotational inertia of the wheels, these equations reduce to

$$\dot{u} = -g (\Lambda_b(\mathbf{s}^*) \cos \theta - \sin \theta), \quad (47)$$

$$0 = \frac{g}{R} (\nu \mu(s_r^*) \lambda_r(\mathbf{s}^*) - \Upsilon_{br}), \quad (48)$$

$$0 = \frac{g}{R} (\nu \mu(s_f^*) \lambda_f(\mathbf{s}^*) - \Upsilon_{bf}). \quad (49)$$

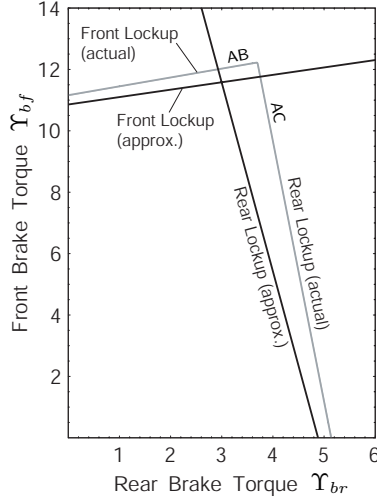


Figure 15. Comparison of the approximate and actual critical brake torques for the two-wheel braking model at which front and rear lockup is guaranteed for $h/l = 0.2$, $c/l = 0.6$, $b/l = 0.4$, $\theta = 0$, and $\nu = 15$. The lines AB and AC correspond to saddle-node bifurcations of the stable node $\mathbf{s}^{(aa)}$ with the saddle points $\mathbf{s}^{(ar)}$ and $\mathbf{s}^{(ra)}$.

The approximations given by Equation (44) follows from solving Equation (48) and Equation (49) for the required brake torques Υ_{bi} and then maximizing the corresponding deceleration of the vehicle (Equation 47) by setting $\mathbf{s}^* = \mathbf{s}_p = (s_p, s_p)$.

A graphical comparison of the approximate (Equation 44) and exact (Equation 45 and Equation 46) results for the front and rear wheel lockup thresholds is shown in Figure 15. It is noted that the approximate results provide conservative estimates for these thresholds, since lockup occurs at values larger than the estimates. The results are reasonably close for typical automobiles.⁸ However, the error may be significant for large-wheeled vehicles. (See Figure 5 for representative results for the single-wheel braking model.)

3.5. STOPPING TIME

Given a set of initial conditions and brake torques, trajectories evolve in the (u, \mathbf{s}) state space according to the equations of motion, which are given by Equation (32). Since $\dot{s}_i \sim \frac{1}{u}$, the time rate of change of slip increases for decreasing u and becomes infinite as $u \rightarrow 0$. Two important consequences of this observation are:

1. The slip dynamics evolve much faster than the speed dynamics (for reasonable speeds u);
2. The vehicle must come to rest under steady slip conditions.

These features enable the stopping time for the two-wheel braking model to be estimated, as was done in Section 2.4.3 for the single-wheel braking model.

A very common situation is for a brake torque pair $\Upsilon_{br} < \Upsilon_{br}^{cr}$ and $\Upsilon_{bf} < \Upsilon_{bf}^{cr}$ to be *suddenly* applied to a vehicle initially moving at a forward speed $u(t=0) = u_o > 0$. Then trajectories evolve

from $(u, s_r, s_f) = (u_o, 0, 0)$, approach the stable invariant manifold, and essentially evolve along $\mathcal{V}_b^{(aa)}$, which is associated with $\mathbf{s}^{(aa)}$. (See Equation 40.) The corresponding vehicle acceleration

$$\dot{u} = -g(\Lambda_b(\mathbf{s}^*) \cos \theta - \sin \theta)$$

is constant and either negative or positive, depending on the sign of $\Lambda_b(\mathbf{s}^*) \cos \theta - \sin \theta$.⁹ The term $g \sin \theta$ is the contribution to the vehicle deceleration (or acceleration) due to the incline and $-g\Lambda_b(\mathbf{s}^*) \cos \theta < 0$ represents the level of deceleration along the inclined surface due to the friction generated at the rear and front tire/road interfaces. The corresponding vehicle speed changes linearly according to the equation

$$u(t) = u_o^{(aa)} - \left(\Lambda_b(\mathbf{s}^{(aa)}) \cos \theta - \sin \theta \right) g \left(t - t^{(aa)} \right), \quad t^{(aa)} \leq t \leq t_s, \quad (50)$$

where $u_o^{(aa)}$ is the vehicle speed at $t = t^{(aa)}$ when the trajectory has essentially reached $\mathcal{V}_b^{(aa)}$. Since $\dot{s}_i \sim \frac{1}{u}$, it follows that $t^{(aa)} \cong 0$ and $u_o^{(aa)} \cong u_o$. If θ and Υ_{bi} are such that $\dot{u} < 0$, that is, if $\Lambda_b(\mathbf{s}^*) \cos \theta - \sin \theta > 0$, then

$$t_s \cong \frac{u_o}{\left(\Lambda_b(\mathbf{s}^{(aa)}) \cos \theta - \sin \theta \right) g} \quad (51)$$

is an estimate of the stopping time, that is, the time it takes for the vehicle speed to reach zero. Its accuracy increases for decreasing initial speed u_o .

4. Conclusions and Directions for Future Work

The formulation presented here provides useful insight into the dynamics of vehicles during braking. In the present study only the case of a vehicle on flat wet or dry pavement was considered, but the formulation allows for more general studies to be carried out. Specifically, the two functions $h_{br}(\mathbf{s})$ and $h_{bf}(\mathbf{s})$ can be generated for a given vehicle, road surface, and incline angle and then used to provide a complete picture of the possible braking conditions that may be encountered as the brake torques are varied. It should be noted that, since the general features of the model are hyperbolic, it is expected that they will remain qualitatively unchanged if one tweaks the model, for example by varying parameters. However, large changes in the model, for example, taking a friction model that is not unimodal, or using an incline sufficiently large such that braking cannot occur, will no doubt change the nature of the bifurcation diagram.

The analysis predicts gross features of the vehicle behavior that would be expected as the brake torques are varied (e.g., as one continues to increase the front brake torque, the front wheels eventually lock up, but will exhibit hysteresis when backing off the brake). More importantly, the analysis allows one to put the complete picture of these behaviors together in a systematic manner from first principles, accounting for the relevant system and environmental parameters. By doing so, it is shown that the interplay between brake torques and wheel behavior can be quite complicated, especially near the region where lockup in both wheels is simultaneously imminent. This is important due to the fact that this is precisely the region where one would like to operate in order to brake aggressively and maintain vehicle stability.

Several topics related to this line of work remain to be considered, including the following:

- investigations into the effects of system parameters, inclines, and friction characteristics using the approach developed herein (for example, a bifurcation analysis in which the incline angle is taken as the parameter);
- the extension of the approach to the case of vehicle acceleration, as was done for the single wheel model [1];
- the possible utility of the results in selecting brake proportioning schedules, wherein the front and rear brake torques are regulated in order to maximum the overall braking force while maintaining vehicle stability [2, 3];
- the effects of cornering on braking and acceleration, wherein a four-wheel model is employed;
- inclusion of the effects of rolling and air resistance on the dynamic model [4];
- the incorporation of these models into ABS/TCS development, where slip plays a central role.

Notes

¹ m represents the entire vehicle mass, including its wheels. The mass of the wheels is assumed to be distributed in the single-wheel model (which is captured by the polar moment of inertia J) and otherwise concentrated at its mass center C .

² It should be noted that the authors reported $\mu(s) : I \mapsto I$ in [1]. While this is not incorrect, and has no effect on the analysis in that study, it is unnecessarily restrictive. There is no need to place an upper bound on $\mu(s)$.

³ The following analysis can be easily generalized to the case of different slip characteristics for the two wheels.

⁴ For an invariant point $\mathbf{s}^{(p,k)}$, p indicates rear-slip stability and k indicates front-slip stability; a denotes stable, or *attracting*, r denotes unstable, or *repelling*, and L denotes lockup.

⁵ Note that the boundary equilibria contained in \mathcal{L}_r are attracting in rear slip and that those contained in \mathcal{L}_f are attracting in front slip.

⁶ The reason that this “corner” differs from the others is that none of the equilibria involved are boundary equilibria.

⁷ It should be noted that the exact location of these lines of bifurcation depends fundamentally on the nature of the friction characteristic, which depends in a complicated way on the road surface and on the properties of the tires.

⁸ The error ranges from approximately 5 to 15% for typical vehicles for which $\nu = 15$.

⁹ If θ is sufficiently large and the brake torques are sufficiently small, it is possible that $\dot{u} > 0$.

Acknowledgements

This research was supported in part by the Department of Applied Mechanics at the Budapest University of Technology and Economics, the Department of Mechanical Engineering & the Institute for Global Engineering Education at Michigan State University, the US-Hungarian Joint Fund for Technological Development, and by a grant from the National Science Foundation. The authors would like to thank Mr. Jeff Rhoads and Professor Brian Feeny of Michigan State University for

their insight and helpful comments. SWS is grateful to the Department of Mechanical Engineering at the University of California-Santa Barbara for their hospitality during a sabbatical visit during which this work was completed.

References

1. B. Olson, S. Shaw, and G. Stépán, “Nonlinear dynamics of vehicle traction,” *Vehicle System Dynamics*, vol. 40, no. 6, pp. 377–399, 2003.
2. T. Gillespie, *Fundamentals of Vehicle Dynamics*. Warrendale: Society of Automotive Engineers (SAE), Inc, 1992.
3. J. Wong, *Theory of Ground Vehicles*. New York: Wiley, 1978.
4. B. Olson, “Nonlinear dynamics of longitudinal ground vehicle traction,” MS thesis, Michigan State University, East Lansing, MI, 2001.
5. SAE Standard, “Antilock brake system review,” *SAE Paper No. Iaa46*, pp. 90–102, 1992.
6. J. Harned, L. Johnston, and G. Scharpf, “Measurement of tire brake force characteristics as related to wheel slip (antilock) control system design,” *SAE Paper No. 690214*, pp. 909–925, 1969.
7. G. Goodenow, T. Kolhoff, and F. Smithson, “Tire-road friction measuring system—a second generation,” *SAE Paper No. 680137*, pp. 571–579, 1968.
8. E. Bakker, L. Nyborg, and H. Pacejka, “Tyre modelling for use in vehicle dynamics studies,” *SAE Paper No. 870421*, pp. 190–204, 1987.
9. E. Bakker, H. Pacejka, and L. Lidner, “A new tire model with and application in vehicle dynamics studies,” *SAE Paper No. 890087*, pp. 101–113, 1989.
10. Y. Liu and J. Sun, “Target slip tracking using gain-scheduling for antilock braking systems,” *Proceedings of the American Control Conference*, vol. 2, pp. 1178–1182, June 1995.
11. S. Strogatz, *Nonlinear Dynamics and Chaos*. Reading: Addison-Wesley, 1994.